WIDEBAND IMPEDANCE MATCHING IN TRANSIENT REGIME OF ACTIVE CIRCUIT USING LOSSY NONUNIFORM MULTICONDUCTOR TRANSMISSION LINES

A. Amharech[*] and H. Kabbaj

Laboratoire LSSC-Equipe de recherche CEM, Faculté des Sciences et Techniques-Fès, Université Sidi Mohamed Ben Abdellah, B.P. 2202-Route d'Imouzzer, FES, Maroc

Abstract—This paper focuses on the electromagnetic compatibility domain, coupling in microwave circuits and wideband (WB) impedance matching in time domain using a purely temporal method, such as the centered-points Finite Difference Time Domain (FDTD). The paper here presents a new approach of WB impedance matching in transient regime and coupling context, of active circuits such as multiple complex nonlinear components (represented here by metal semiconductor field-effect transistors (MESFETs)), using Nonuniform Multiconductor Transmission Lines (NMTL) with frequency dependent losses and FDTD as modeling method. The FDTD method has several positive aspects such as the ease to introduce nonlinear components in the algorithm, the ease to use NMTL and the gain in simulation time and memory space. Also the FDTD method allows the study of WB impedance matching in time domain without recourse to the frequency domain. Systematic comparisons of the results of this method with those obtained by PSpice are done to validate this study. These comparisons show a good agreement between the method presented here and PSpice. The technique presented in this paper shows higher efficiency and ease to implement when compared to PSpice in regard to the treatment of frequency dependent losses, or shapes of transmission lines.

1. INTRODUCTION

Impedance matching is a very important concept in telecommunications and microwave domain. To obtain the best performance of the circuits, it cannot be ignored. There are many techniques used to match loads to sources, such as the use of single stub, multi-stubs, uniform transmission line, sections of quarter-wave uniform transmission lines, tapered transmission line, or nonuniform and arbitrary nonuniform transmission line for matching impedance in narrow or wide band frequency [1–6]. These techniques are usually used in the frequency domain and in non coupling context, just for single load as in [5, 7]. This is no longer the case today where the trend is towards integration of circuits and the context in which the coupling between the circuits can no longer be ignored.

With the development of numerical data communications, the demand of high speed and wide-band circuit increases rapidly [7–11]. For these reasons the study of the transient domain of components is becoming more important, specifically for the microwave components like MESFETs and their matching circuits taking into consideration frequency dependent losses and the nonlinear operation of the transistors.

This paper presents a technique that uses regular NMTL with frequency dependent losses to achieve a WB impedance matching of multi-MESFETs inputs in transient domain. The study is based on FDTD method and the multi-MESFETs are modeled by their large signal scheme.

2. ANALYSIS OF NMTL USING THE FDTD METHOD

Under the assumption of a TEM field structure and in the absence of external electromagnetic field, the MTL with frequency dependent losses can be described, in time domain, by a system of partial differential equations as:

$$\frac{\partial}{\partial z}\mathbf{V}\left(z,t\right) + \mathbf{Z}_{int}\left(t\right) * \mathbf{I}\left(z,t\right) + \mathbf{L}\frac{\partial}{\partial t}\mathbf{I}\left(z,t\right) = 0, \tag{1}$$

$$\frac{\partial}{\partial z}\mathbf{I}\left(z,t\right) + \mathbf{G}\left(t\right) * \mathbf{V}\left(z,t\right) + \mathbf{C}\frac{\partial}{\partial t}\mathbf{V}\left(z,t\right) = 0, \tag{2}$$

where $*$ is the convolution product.

In the case of NMTL, the line is divided into multiple segments, of different sections (Figure 1). Each segment has its own distributed parameters (they can change from one segment to another).
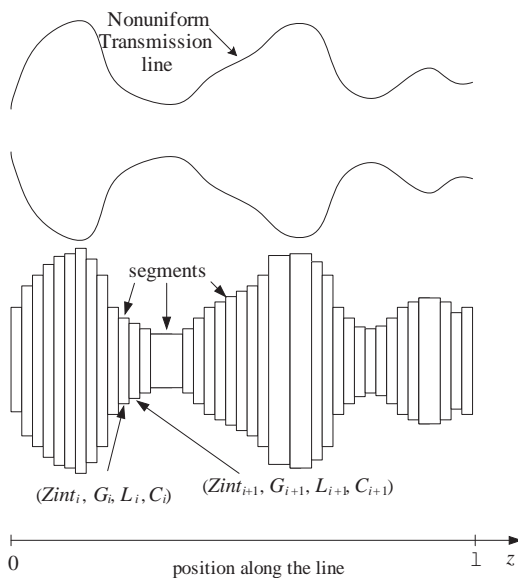
Figure 1. Model of a nonuniform transmission line.

This leads to the new system of equations, where the parameters $\mathbf{Z}_{int}$, $\mathbf{L}$, $\mathbf{C}$ and $\mathbf{R}$ depend on the position z along the line:

$$\frac{\partial}{\partial z}\mathbf{V}(z,t) + \mathbf{Z}_{int}(z,t) * \mathbf{I}(z,t) + \mathbf{L}(z)\frac{\partial}{\partial t}\mathbf{I}(z,t) = 0, \qquad (3)$$

$$\frac{\partial}{\partial z}\mathbf{I}(z,t) + \mathbf{G}(z,t) * \mathbf{V}(z,t) + \mathbf{C}(z)\frac{\partial}{\partial t}\mathbf{V}(z,t) = 0. \qquad (4)$$

The $N \times 1$ vectors $\mathbf{V}$ and $\mathbf{I}$ contain the N lines voltages as $[\mathbf{V}(z,t)]_i = V_i(z,t)$ and the N lines currents as $[\mathbf{I}(z,t)]_i = I_i(z,t)$, where the entry in the ith row of a vector $\mathbf{V}$ is denoted as $[\mathbf{V}]_i$, z is the position along the line, t denotes time.

The $N \times N$ matrices $\mathbf{Z}_{int}$, $\mathbf{L}$, $\mathbf{C}$ and $\mathbf{G}$ are the per-unit length, conductor internal impedance, inductance, capacitance, and conductance describing the MTL. In the case of a uniform line, the internal impedance contains both resistance and internal inductance (due to the magnetic flux in the conductors) as $Z_{int}(s) = R + sL_{int}(s)$. In general, the impedance is a nonlinear function of frequency. Thus, the description of the frequency dependent loss is introduced by using the widely used Nahman approximation of the internal impedance $Z_{int}(s) = A + B\sqrt{s}$ as in [12] and Qingjian formulation of conductance $G(s) = G^{dc} + G^{df}\frac{s}{(s+1/\tau_p)}$ as in [13], where s is the Laplace transform variable.

Where, for NMTL:

$$\mathbf{A}(z) = \frac{1}{\sigma_m \mathbf{w}(z) t_m}, \quad \mathbf{B}(z) = \frac{\sqrt{\frac{\mu}{\sigma}}}{2(\mathbf{w}(z) + t_m)}, \quad \mathbf{G}^{dc}(z) = \frac{\sigma_{di}}{\varepsilon} \mathbf{C}(z), \quad (5)$$

where σ_m is the conductors conductivity, t_m is the conductors thickness, $\mathbf{w}(z)$ is the conductors width along the line, σ_{di} is the dielectric conductivity, μ is the permeability, ε is the permittivity and τ_p is the time constant characteristic of the dielectric substrate.

In the time domain, the dc portion of the impedance ($\mathbf{A}(z)$) affects the late-time response whereas the high-frequency portion ($\mathbf{B}(z)$) affects the early-time response. In order to adequately characterize the NMTL, both portions should be included.

In time domain and according to the expression of Z_{int} in [12], the convolution product $\mathbf{Z}_{int}(z,t) * \mathbf{I}(z,t)$ becomes:

$$\mathbf{Z}_{int}(z,t) * \mathbf{I}(z,t) = Lap^{-1}(\mathbf{Z}_{int}(z,s)\mathbf{I}(z,s))$$
$$= Lap^{-1}\left(\mathbf{A}(z)\mathbf{I}(z,s) + \mathbf{B}(z)\frac{1}{\sqrt{s}}s\mathbf{I}(z,s)\right). \quad (6)$$

Knowing that $Lap^{-1}(\frac{1}{\sqrt{s}}) = \frac{1}{\sqrt{\pi t}}$, $\mathbf{Z}_{int}(z,t) * \mathbf{I}(z,t)$ of Equation (6) becomes:

$$\mathbf{Z}_{int}(z,t) * \mathbf{I}(z,t) = \mathbf{A}(z)\mathbf{I}(z,t) + \frac{\mathbf{B}(z)}{\sqrt{\pi}}\int_0^t \frac{1}{\sqrt{\tau}}\frac{\partial \mathbf{I}(z,t-\tau)}{\partial(t-\tau)}d\tau. \quad (7)$$

Also, in time domain and according to the expression of G in [13], the convolution product $\mathbf{G}(z,t) * \mathbf{V}(z,t)$ becomes:

$$\mathbf{G}(z,t) * \mathbf{V}(z,t) = Lap^{-1}(\mathbf{G}(z,s)\mathbf{V}(z,s))$$
$$= Lap^{-1}\left(\mathbf{G}^{dc}(z)\mathbf{V}(z,s) + \mathbf{G}^{df}(z)\frac{1}{\left(s+\frac{1}{\tau_p}\right)}s\mathbf{V}(z,s)\right). \quad (8)$$

Therefore,

$$\mathbf{G}(z,t) * \mathbf{V}(z,t) = \mathbf{G}^{dc}(z)\mathbf{V}(z,t) + \mathbf{G}^{df}(z)\int_0^t e^{-\tau/\tau_p}\frac{\partial \mathbf{V}(z,t-\tau)}{\partial(t-\tau)}d\tau. \quad (9)$$

The FDTD method is widely used in solving various kinds of electromagnetic problems wherein lossy, nonlinear, and/or non homogeneous media may be considered.

In order to evaluate voltages and currents along the transmission line, NMTL Equations (3) and (4) are translated into finite-difference expressions. The line axis z is divided into ndz cells, each of equal length Δz and the time variable t in ndt segments of equal length Δt.
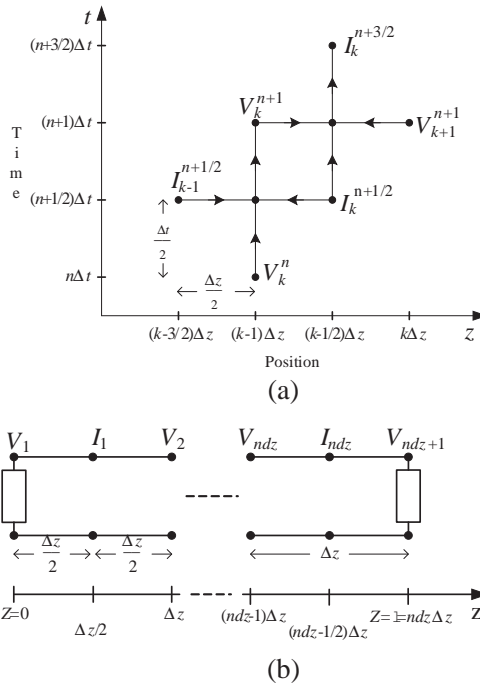
Figure 2. Illustration of (a) the FDTD discretization of the voltages and currents along the MTL and (b) the locations of the solution variables on the line.

In order to ensure stability in the FDTD solution of the MTL equations, the discrete voltage and current solution points are not located at the same point; they are interlaced. Each voltage and adjacent current solution point are separated by $\Delta z/2$. In addition, the discrete voltages and currents must be similarly interlaced in time with the time points for the voltages and for the currents being spaced by $\Delta t/2$ [14] as illustrated in Figure 2.

The use of the second order central differences according to the scheme in Figure 2(a) to discretize the derivatives in the NMTL, and according to Nahman approximation of $\mathbf{Z}_{int}$ and Qingjian formulation of $\mathbf{G}$ and to Equations (7) and (9), Equations (3) and (4) leads to the recursive formula for interior point:

$$\frac{1}{\Delta z}\left[\mathbf{V}_{k+1}^{n+1}-\mathbf{V}_{k}^{n+1}\right]+\frac{1}{\Delta t}\mathbf{L}_k\left[\mathbf{I}_{k}^{n+\frac{3}{2}}-\mathbf{I}_{k}^{n+\frac{1}{2}}\right]+\frac{1}{2}\mathbf{A}_k\left[\mathbf{I}_{k}^{n+\frac{3}{2}}+\mathbf{I}_{k}^{n+\frac{1}{2}}\right]$$

$$+\frac{1}{2}\frac{\mathbf{B}_k}{\sqrt{\pi\Delta t}}\sum_{m=0}^{n}\left[\mathbf{I}_{k}^{n+\frac{3}{2}-m}-\mathbf{I}_{k}^{n+\frac{1}{2}-m}\right]\int_{m}^{(m+1)}\frac{d\tau}{\tau}=0, \qquad (10)$$

and

$$\frac{1}{\Delta z}\left[\mathbf{I}_k^{n+1/2}-\mathbf{I}_{k-1}^{n+1/2}\right]+\frac{1}{\Delta t}\mathbf{C}_k\left[\mathbf{V}_k^{n+1}-\mathbf{V}_k^n\right]+\frac{1}{2}\mathbf{G}_k^{dc}\left[\mathbf{V}_k^{n+1}+\mathbf{V}_k^n\right]$$

$$+\mathbf{G}_k^{df}\sum_{m=0}^{n}\left[V_k^{n+1-m}-V_k^{n-m}\right]\int_m^{(m+1)}e^{-\frac{\Delta t}{\tau_p}\tau}d\tau=0. \qquad (11)$$

Thus

$$\mathbf{I}_k^{n+3/2}=\mathbf{D}_k\mathbf{E}_k\mathbf{I}_k^{n+1/2}+\frac{\mathbf{D}_k}{\Delta z}\left(\mathbf{V}_k^{n+1}-\mathbf{V}_{k+1}^{n+1}\right)-\frac{\Delta z}{\sqrt{\pi\Delta t}}\mathbf{D}_k\mathbf{B_k}\mathbf{T}_k^n,$$

$$\text{where } k=1,2,\ldots,ndz. \qquad (12)$$

$$\mathbf{D}_k=\left(\frac{\mathbf{L}_k}{\Delta t}+\frac{\mathbf{A}_k}{2}+\frac{2\mathbf{B}_k}{\sqrt{\pi\Delta t}}\right)^{-1}, \qquad (13)$$

$$\mathbf{E}_k=\frac{\mathbf{L}_k}{\Delta t}-\frac{\mathbf{A}_k}{2}+\frac{2\mathbf{B}_k}{\sqrt{\pi\Delta t}}, \qquad (14)$$

$$\mathbf{T}_k^n=\sum_{m=1}^{n}\left[\mathbf{I}_k^{n+\frac{3}{2}-m}-\mathbf{I}_k^{n+\frac{1}{2}-m}\right]\int_m^{(m+1)}\frac{d\tau}{\tau}, \qquad (15)$$

and

$$\mathbf{V}_k^{n+1}=\mathbf{M}_k\mathbf{N}_k\mathbf{V}_k^n+\frac{\mathbf{M}_k}{\Delta z}\left(\mathbf{I}_{k-1}^{n+\frac{1}{2}}-\mathbf{I}_k^{n+\frac{1}{2}}\right)-\mathbf{M}_k\mathbf{G}_k^{df}\sum_{m=1}^{n}$$

$$\left[\mathbf{V}_k^{n+1-m}-\mathbf{V}_k^{n-m}\right]f(m), \text{ where } k=1,2,\ldots,ndz+1. \qquad (16)$$

$$\mathbf{M}_k=\left(\frac{1}{2\Delta t}(\mathbf{C}_k+\mathbf{C}_{k-1})+\frac{1}{4}\left(\mathbf{G}_k^{dc}+\mathbf{G}_{k-1}^{dc}\right)+\frac{1}{2}\left(\mathbf{G}_k^{df}+\mathbf{G}_{k-1}^{df}\right)f(0)\right)^{-1}, (17)$$

$$\mathbf{N}_k=\frac{1}{2\Delta t}(\mathbf{C}_k+\mathbf{C}_{k-1})-\frac{1}{4}\left(\mathbf{G}_k^{dc}+\mathbf{G}_{k-1}^{dc}\right)+\frac{1}{2}\left(\mathbf{G}_k^{df}+\mathbf{G}_{k-1}^{df}\right)f(0), (18)$$

$$f(m)=\int_m^{(m+1)}e^{-\frac{\Delta t}{\tau_p}\tau}d\tau \qquad (19)$$

$$f(0)=\int_0^1 e^{-\frac{\Delta t}{\tau_p}\tau}d\tau \qquad (20)$$

Incorporating boundary conditions for $k=1$ (in the source) and $k=ndz+1$ (in the load), leads to:

$$\mathbf{V}_1^{n+1}=\mathbf{P}_1\mathbf{Q}_1\mathbf{V}_1^n+\frac{2}{\Delta z}\mathbf{P}_1\left(\mathbf{R}_s^{-1}\frac{\mathbf{V}_s^{n+1}+\mathbf{V}_s^n}{2}-\mathbf{I}_1^{n+1/2}\right)$$

$$-\mathbf{P}_1\mathbf{G}_1^{df}\sum_{m=1}^{n}\left[\mathbf{V}_1^{n+1-m}-\mathbf{V}_1^{n-m}\right]f(m), \qquad (21)$$

$$\mathbf{V}_{ndz+1}^{n+1} = \mathbf{P}_{ndz+1}\mathbf{Q}_{ndz+1}\mathbf{V}_{ndz+1}^{n} + \frac{2\mathbf{P}_{ndz+1}}{\Delta z}\left(\mathbf{I}_{ndz}^{n+1/2} - \frac{\mathbf{I}_{L}^{n+1}+\mathbf{I}_{L}^{n}}{2}\right)$$

$$-\mathbf{P}_{ndz+1}\mathbf{G}_{ndz+1}^{df}\sum_{m=1}^{n}\left[\mathbf{V}_{ndz+1}^{n+1-m} - \mathbf{V}_{ndz+1}^{n-m}\right]f(m), \quad (22)$$

where

$$\mathbf{P}_1 = \left(\frac{\mathbf{C}_1}{\Delta t} + \frac{\mathbf{G}_1^{dc}}{2} + \mathbf{G}_1^{df}f(0) + \mathbf{R}_s^{-1}\right)^{-1}, \quad (23)$$

$$\mathbf{Q}_1 = \left(\frac{\mathbf{C}_1}{\Delta t} - \frac{\mathbf{G}_1^{dc}}{2} + \mathbf{G}_1^{df}f(0) - \mathbf{R}_s^{-1}\right), \quad (24)$$

$$\mathbf{P}_{ndz+1} = \left(\frac{\mathbf{C}_{ndz+1}}{\Delta t} + \frac{\mathbf{G}_{ndz+1}^{dc}}{2} + \mathbf{G}_{ndz+1}^{df}f(0)\right)^{-1}, \quad (25)$$

$$\mathbf{Q}_{ndz+1} = \frac{\mathbf{C}_{ndz+1}}{\Delta t} - \frac{\mathbf{G}_{ndz+1}^{dc}}{2} + \mathbf{G}_{ndz+1}^{df}f(0), \quad (26)$$

and

$$\mathbf{V}_k^n \equiv \mathbf{V}\left[(k-1)\Delta z, n\Delta t\right], \quad (27)$$
$$\mathbf{I}_k^n \equiv \mathbf{I}\left[(k-1/2)\Delta z, n\Delta t\right]. \quad (28)$$

For the stability of the FDTD relations, the time step Δt must respect the Courant condition [15]. Therefore Δt must be equal to or less than the $v_{p\,\mathrm{max}}$ (Equation (29)). Where $v_{p\,\mathrm{max}}$ is the largest phase velocity found in the propagation along the line.

$$\Delta t \leq \frac{\Delta z}{v_{p\,\mathrm{max}}}. \quad (29)$$

In the case of linear loads (resistance), $\mathbf{V}_{ndz+1} = \mathbf{V}_L = \mathbf{R}_L \cdot \mathbf{I}_L$. Thus the Equation (22) becomes:

$$\mathbf{V}_{ndz+1}^{n+1} = \mathbf{O}_{ndz+1}\mathbf{X}_{ndz+1}\mathbf{V}_{ndz+1}^{n} + \frac{2\mathbf{O}_{ndz+1}}{\Delta z}\mathbf{I}_{ndz}^{n+1/2}$$

$$-\mathbf{O}_{ndz+1}\mathbf{G}_{ndz+1}^{df}\sum_{m=1}^{n}\left[\mathbf{V}_{ndz+1}^{n+1-m} - \mathbf{V}_{ndz+1}^{n-m}\right]f(m), \quad (30)$$

where

$$\mathbf{O}_{ndz+1} = \left(\frac{\mathbf{C}_{ndz+1}}{\Delta t} + \frac{\mathbf{G}_{ndz+1}^{dc}}{2} + \mathbf{G}_{ndz+1}^{df}f(0) + \frac{1}{\Delta z}\mathbf{R}_L^{-1}\right)^{-1}, \quad (31)$$

$$\mathbf{X}_{ndz+1} = \frac{\mathbf{C}_{ndz+1}}{\Delta t} - \frac{\mathbf{G}_{ndz+1}^{dc}}{2} + \mathbf{G}_{ndz+1}^{df}f(0) - \frac{1}{\Delta z}\mathbf{R}_L^{-1}. \quad (32)$$

When the transmission lines are connected by nonlinear loads, the above method may be similarly implemented and there is no change in the topological equations since the KVL and KCL equations are independent of the branch relations. The current load ($\mathbf{I}_L$) in Equation (22) is replaced by its nonlinear expression according to the nonlinear load.

The solution of these equations starts with an initially relaxed line having zero voltages and currents values. First voltages along the line are solved for a fixed time from Equation (16) in terms of the previous solutions, and then currents are solved from Equation (12) in terms of these and previous values.

3. EQUATIONS AT THE ENDPOINTS OF NMTL FOR NONLINEAR LOADS

Here the NMTL treated are loaded by multi-MESFETs, in a common-source configuration. The interest is focused on the nonlinear behavior of the transistor MESFET. Hence, as in [16] for single transistor, but without taking into account the gate resistance, or as in [17] for the case of multi-transistors, the intrinsic large signal equivalent scheme of the MESFET is adopted (Figure 3). It is taken from [18].

Where

$$
\begin{aligned}
&\mathbf{C}_{gs}(\mathbf{V}_g(t)) \\
&= \begin{cases} \mathbf{C}_{gs_0}\left(\sqrt{1-\left(\mathbf{V}_b^{-1}\mathbf{V}_g(t)\right)}\right)^{-1}, & \text{for } \mathbf{V}_g < (F_C.\mathbf{V}_b) \\ \dfrac{\mathbf{C}_{gs_0}}{(1-F_C)^{\frac{3}{2}}}\left(1-\frac{3}{2}F_C+\frac{1}{2}\mathbf{V}_b^{-1}\mathbf{V}_g(t)\right), & \text{for } \mathbf{V}_g \geq (F_C.\mathbf{V}_b) \end{cases}
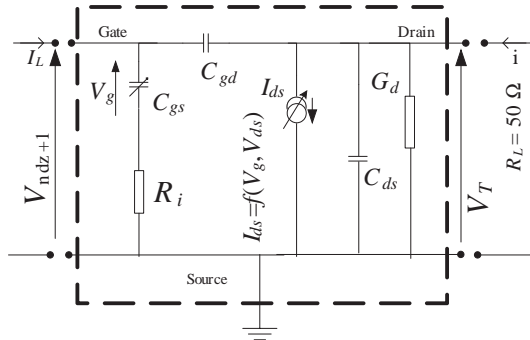\end{aligned} \tag{33}
$$

Figure 3. Configuration of the end of NMTL loaded by a MESFET (the intrinsic large-signal model of a MESFET is in the dashed square).

$$\mathbf{I}_{ds}(\mathbf{V}_g(t), \mathbf{V}_{ds}(t))$$
$$= \left(\mathbf{A}_0\boldsymbol{\delta} + \mathbf{A}_1\mathbf{V}_g(t) + \mathbf{A}_2\mathbf{V}_g(t)^2 + \mathbf{A}_3\mathbf{V}_g(t)^3\right)\tanh\left(\boldsymbol{\alpha}\mathbf{V}_{ds}(t)\right), \quad (34)$$

where $\mathbf{V}_b$ is the built-in potential of the Schottky gate, F_C is forward bias depletion capacitance coefficient and $\boldsymbol{\delta}$ is a $(N \times 1)$ vector of 1.

The expressions taken from [18, 19] are scalars and are written to describe a single transistor. In this study several transistors are simultaneously treated. So for that, these expressions were developed to describe multi-transistors. Scalars are now $(N \times 1)$ vectors for voltages and currents, and $(N \times N)$ matrices for the transistors parameters. Where N is the number of transistors treated.

From Figure 3 (as in [17]) and in terms of finite differences, the expression of $\mathbf{I}_L^{n+1}$, $\mathbf{V}_{ndz+1}^{n+1}$ and $\mathbf{V}_T^{n+1}$ are extracted and are:

$$\mathbf{V}_T^{n+1} = -\mathbf{R}_L\left(\mathbf{C}_{ds}\left[\frac{\mathbf{V}_T^{n+1} - \mathbf{V}_T^n}{\Delta t}\right] - \mathbf{C}_{gd}\left[\frac{\mathbf{V}_{ndz+1}^{n+1} - \mathbf{V}_{ndz+1}^n}{\Delta t} - \frac{\mathbf{V}_T^{n+1} - \mathbf{V}_T^n}{\Delta t}\right]\right.$$
$$+ \mathbf{G}_d\mathbf{V}_T^{n+1} + \left(\mathbf{A}_0\boldsymbol{\delta} + \mathbf{A}_1\mathbf{V}_g^{n+1} + \mathbf{A}_2\mathbf{V}_g^{n+1^2} + \mathbf{A}_3\mathbf{V}_g^{n+1^3}\right)$$
$$\left. \tanh\left(\boldsymbol{\alpha}\mathbf{V}_T^{n+1}\right)\right) \qquad (35)$$

$$\mathbf{I}_L^{n+1} = \mathbf{C}_{gs}\left(\mathbf{V}_g^{n+1}\right)\left[\frac{\mathbf{V}_g^{n+1} - \mathbf{V}_g^n}{\Delta t}\right] + \frac{\mathbf{C}_{gd}}{\Delta t}\left[-\mathbf{V}_{ndz+1}^n - \mathbf{V}_T^{n+1} + \mathbf{V}_T^n\right]$$
$$+ \frac{\mathbf{C}_{gd}}{\Delta t}\left[\mathbf{V}_g^{n+1} + \mathbf{R}_i\mathbf{C}_{gs}\left(\mathbf{V}_g^{n+1}\right)\left[\frac{\mathbf{V}_g^{n+1} - \mathbf{V}_g^n}{\Delta t}\right]\right], \qquad (36)$$

$$\mathbf{V}_{ndz+1}^{n+1} = \mathbf{V}_g^{n+1} + \mathbf{R}_i\mathbf{C}_{gs}\left(\mathbf{V}_g^{n+1}\right)\left[\frac{\mathbf{V}_g^{n+1} - \mathbf{V}_g^n}{\Delta t}\right]. \qquad (37)$$

Replacing $\mathbf{I}_L^{n+1}$ of Equation (36) and $\mathbf{V}_{ndz+1}^{n+1}$ of Equation (37) in Equation (22) leads to a new equation relating $\mathbf{V}_g^{n+1}$ and $\mathbf{V}_T^{n+1}$.

With the combination of the new equation relating $\mathbf{V}_g^{n+1}$ and $\mathbf{V}_T^{n+1}$ and the Equation (35), a new system of equations is obtained, from which the values of $\mathbf{V}_g^{n+1}$ and $\mathbf{V}_T^{n+1}$ are deduced. Once $\mathbf{V}_g^{n+1}$ and $\mathbf{V}_T^{n+1}$ are determined, the value of $\mathbf{V}_{ndz+1}^{n+1}$ is deduced.

To solve this new obtained system of equations, where the only unknown term is $\mathbf{V}_g^{n+1}$, the use of the Newton-Raphson method as shown below is required:

$$\mathbf{H} \equiv -\mathbf{V}_g^{n+1} + f\left(\mathbf{V}_g^{n+1}\right) = 0, \qquad (38)$$

where f is a term of $\mathbf{V}_g^{n+1}$ and where the nonlinear components are collected.

The matrix $\mathbf{V}_g^{n+1}$ is found by solving the following equation:

$$\left(\mathbf{V}_g^{n+1}\right)^{m+1} = \left(\mathbf{V}_g^{n+1}\right)^m - \left(\mathbf{J_H}\right)^{-1}\mathbf{H}, \tag{39}$$

where

$$\mathbf{J_H} = \frac{d\mathbf{H}}{d\mathbf{V}_g}|\mathbf{V}_g = \left(\mathbf{V}_g\right)^m. \tag{40}$$

Once $\mathbf{V}_g^{n+1}$ found, $\mathbf{V}_T^{n+1}$ can be determined and thereafter $\mathbf{V}_{ndz+1}^{n+1}$.

The expressions of $\mathbf{V}_T$, $\mathbf{I}_L$ and $\mathbf{V}_{ndz+1}$ in Equations (35), (36) and (37) are originally scalars according to Figure 3 and to the expressions of nonlinear elements taken from [18, 19]. They are developed to $(N{\times}1)$ vectors (where N is the number of conductors or transistors in the line) to describe a system of multiconductor transmission line loaded by multi MESFETs.

4. NUMERICAL EXAMPLES

The study is focused on the wide band impedance matching of the multi MESFETs in time domain using NMTL. It is based on the use of tapered lines.

For that and as an application of NMTL, the NMTL (Figure 4) whose section and characteristic impedance change continuously, is chosen. This structure of NMTL, which consists of triangular NMTL, allows to go, gradually, from one impedance to another while avoiding reflections.
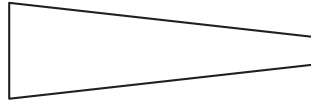

Figure 4. Triangular NMTL used to implement the wideband impedance matching of the multi-MESFETs inputs.

For the numerical examples two cases of loads are chosen: linear loads as resistances and nonlinear loads as MESFET transistors.

4.1. First Example

For the first example, the system as shown in Figure 5 is considered. This example is considered to validate our study in the linear case. The input source is a ramp of $0.5\,\mathrm{V}$ in amplitude, with a rise time of $100\,\mathrm{ps}$. The length of the line is $2\,\mathrm{cm}$.

W_{st}, W_{end}, S_{st} and S_{end} are the dimensions of the conductors' line. They are chosen to obtain the required characteristic impedance in the

beginning and in the end of the line. In this example the beginning characteristic impedance of the line should be $50\,\Omega$. Gradually, an impedance of $100\,\Omega$ is reached (line's end characteristic impedance).

The results of this configuration are compared to those of a mismatched case, where the line is uniform. The length of the line is $2\,\text{cm}$ and is loaded by a resistance of $100\,\Omega$. The parameters of this line are $C = 50.6280e^{-12}\,\text{F/m}$ and $L = 2.10418e^{-6}\,\text{H/m}$, which gives a characteristic impedance of $204\,\Omega$.

The comparison between Figure 6 and Figure 7 shows that the settling time of mismatched circuit $(1.2\,\text{ns})$ is bigger than the matched
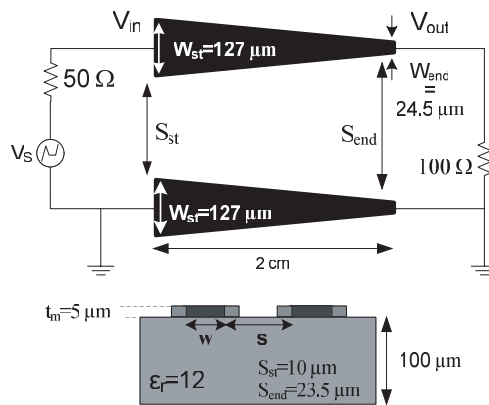
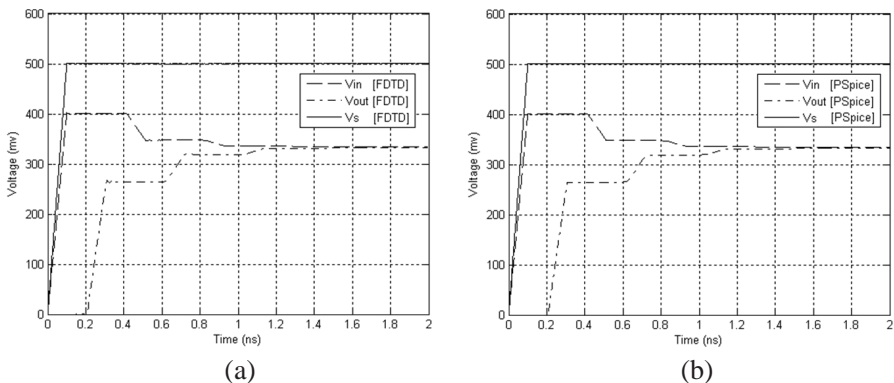**Figure 5.** Configuration of a WB impedance matching in transient domain of a resistance using NMTL.

Figure 6. Input and output voltage for mismatched circuit (uniform transmission line). (a) FDTD. (b) PSpice.

one (0.4 ns). Also, the matcher circuit eliminates overshoot and the distortions, due to the elimination of reflections.

4.2. Second Example

In the second example, the system as shown in Figure 8 is considered. The transistor is in common-source configuration. The input source is a ramp of 0.5 V in amplitude, with a rise time of 100 ps. The length of the line is 2.2 cm.

The parameters of the transistor are shown below:

$C_{gs0} = 2$ pF, $C_{ds} = 0.6$ pF, $C_{gd} = 1.5$ pF, $R_i = 1\,\Omega$, $G_d = 0.2$ mS, $V_b = 0.7$ V, $\alpha = 1.6$, $A_0 = 0.001043$, $A_1 = 0.0011745$, $A_2 =$
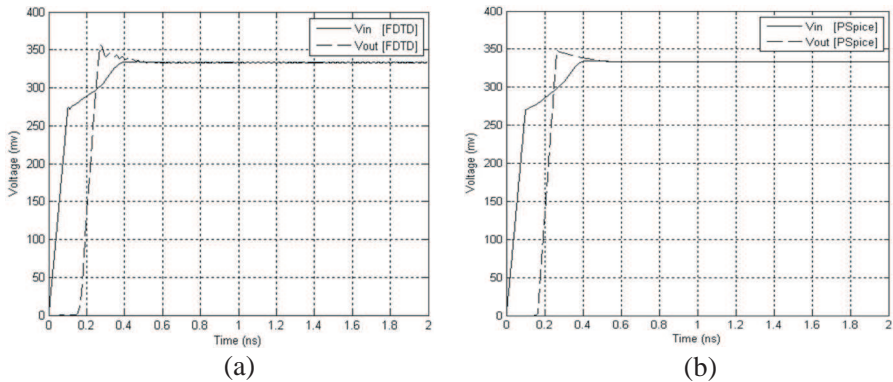
Figure 7. Input and output voltage for WB matched circuit in transient regime. (a) FDTD. (b) PSpice.
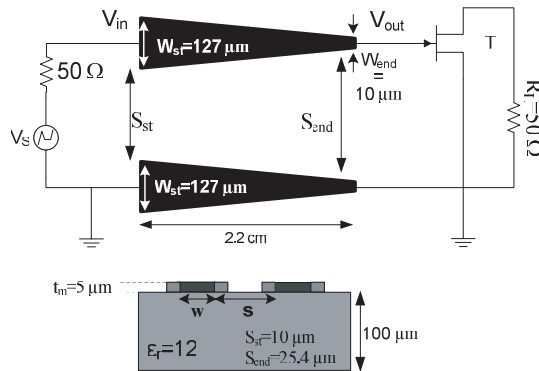
Figure 8. Configuration of a WB impedance matching in transient domain of a non linear MESFET using NMTL.
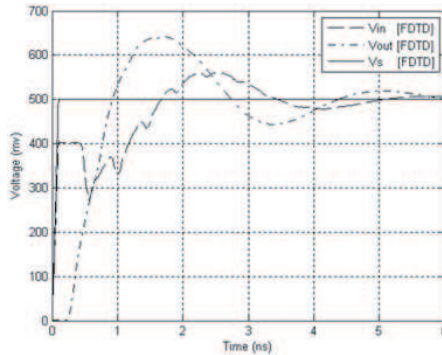
Figure 9. Input and output voltages in the case of mismatch circuit loaded by a MESFET (FDTD).
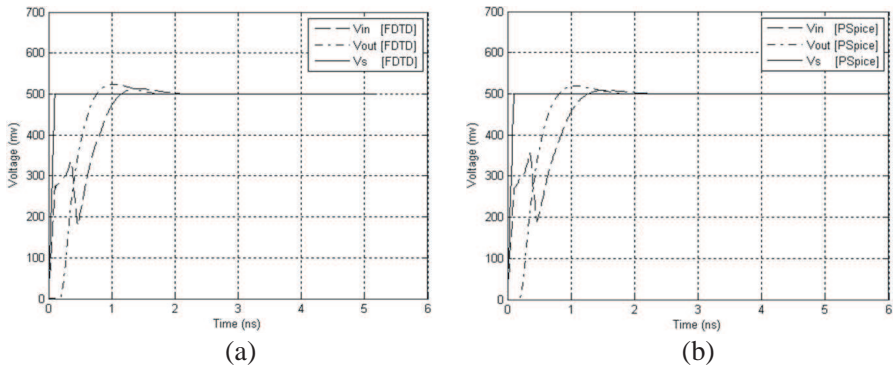

Figure 10. Input and output voltages in the case of WB matched circuit loaded by MESFET. (a) FDTD and (b) PSpice.

-0.0001274, $A_3 = -0.001$, $F_C = 0.5$.

The input resistance of the MESFET was measured by a Time Domain Reflectometer (TDR) and is equal to $125\,\Omega$.

In this example the beginning characteristic impedance of the line should be $50\,\Omega$. Gradually, an impedance of $125\,\Omega$ is reached (line's end characteristic impedance). This impedance corresponds to the MESFET input impedance, as measured by the TDR.

The results of this configuration are compared to those of a mismatched case, where the line is uniform with a characteristic impedance of $204\,\Omega$. The length of the line is $2.2\,\text{cm}$ and is also loaded by a transistor with the same parameters.

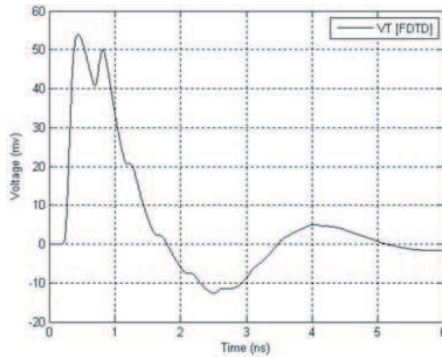The comparison between Figure 9, and Figure 10 on the one hand

Figure 11. Transistor output voltage in the case of mismatched circuit loaded by MESFET (FDTD).

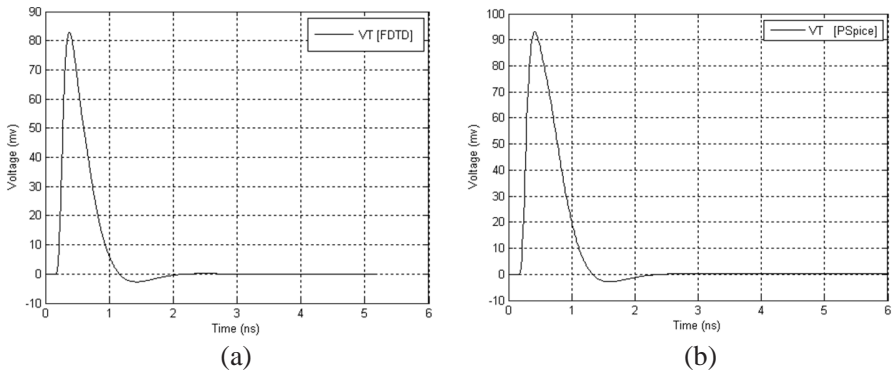|	
(a)	(b)

Figure 12. Transistor output voltage in the case of matched circuit loaded by MESFET. (a) FDTD and (b) PSpice.

and Figure 11 and Figure 12 on the other, shows that the settling time of mismatched circuit (>5 ns) is bigger than the matched one (1.5 ns). Also, the matcher circuit eliminates overshoot and the distortions, due to the elimination of reflections and increased the output voltage of the matched transistor from approximately 55 mV to about 85 mV.

4.3. Third Example

In the third example, the system as shown in Figure 13 is considered. The transistors are in common-source configuration. The input source is a ramp of 0.5 V in amplitude, with a rise time of 100 ps.

The line is composed of five conductors, plus the reference conductor. The length of the line is 2 cm.

Two cases are treated: lossless line and lossy one.

For the case of line with frequency dependent losses:

$$\sigma_{di} = 0.02\,\text{S/m, and } \mathbf{G}^{df} = 20\rceil\tfrac{\text{mS}}{\text{m}}, \text{ where } \rceil = \begin{pmatrix} 1 & 0 & 0 & 0 & 0 \\ 0 & 1 & 0 & 0 & 0 \\ 0 & 0 & 1 & 0 & 0 \\ 0 & 0 & 0 & 1 & 0 \\ 0 & 0 & 0 & 0 & 1 \end{pmatrix}$$

is the identity matrix.

The parameters of the transistors are shown below:

$\mathbf{C}_{gs0} = 2\rceil\,\text{pF}$, $\mathbf{G}_d = 0.2\rceil\,\text{mS}$, $\mathbf{C}_{ds} = 0.6\rceil\,\text{pF}$, $\mathbf{C}_{gd} = 1.5\rceil\,\text{pF}$, $\mathbf{R}_i = 1\rceil\,\Omega$, $\mathbf{V}_b = 0.7\rceil\,\text{V}$, $\boldsymbol{\alpha} = 1.6\rceil$, $\mathbf{A}_0 = 0.001043\rceil$, $\mathbf{A}_1 = 0.0011745\rceil$, $\mathbf{A}_2 = -0.0001274\rceil$, $\mathbf{A}_3 = 0.001\rceil$, $F_C = 0.5$.

The MESFETs used here are identical to the one used in the second example. Therefore, each one has $125\,\Omega$ in the input impedance.

In the case of lossless NMTL, results are shown in Figure 14.

For the case of NMTL with frequency dependent losses, obtained results are shown in the Figure 15.

As in the first example and in the second one, Figure 14 and Figure 15 show that the WB impedance transformer circuit eliminates overshoot and the distortions, due to the elimination of reflections. With this matched circuit, a short settling time (1.5 ns) is obtained, compared to the one of mismatched circuit (> 5 ns), the cancellation of the distortions and the overshoot.

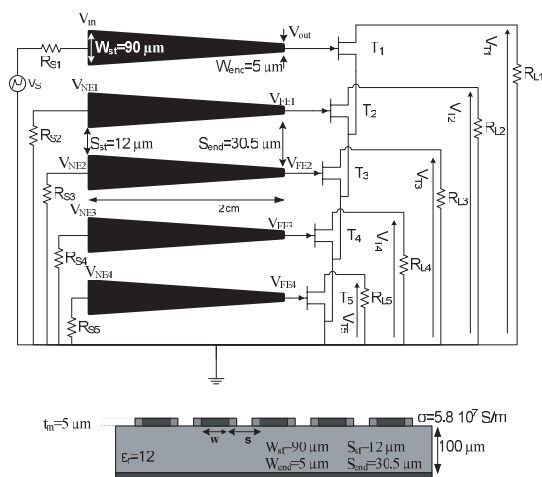The dimensions of the triangular NMTL in case of one conductor

Figure 13. Configuration of a WB impedance matching in transient regime of a nonlinear multi-MESFET using NMTL.
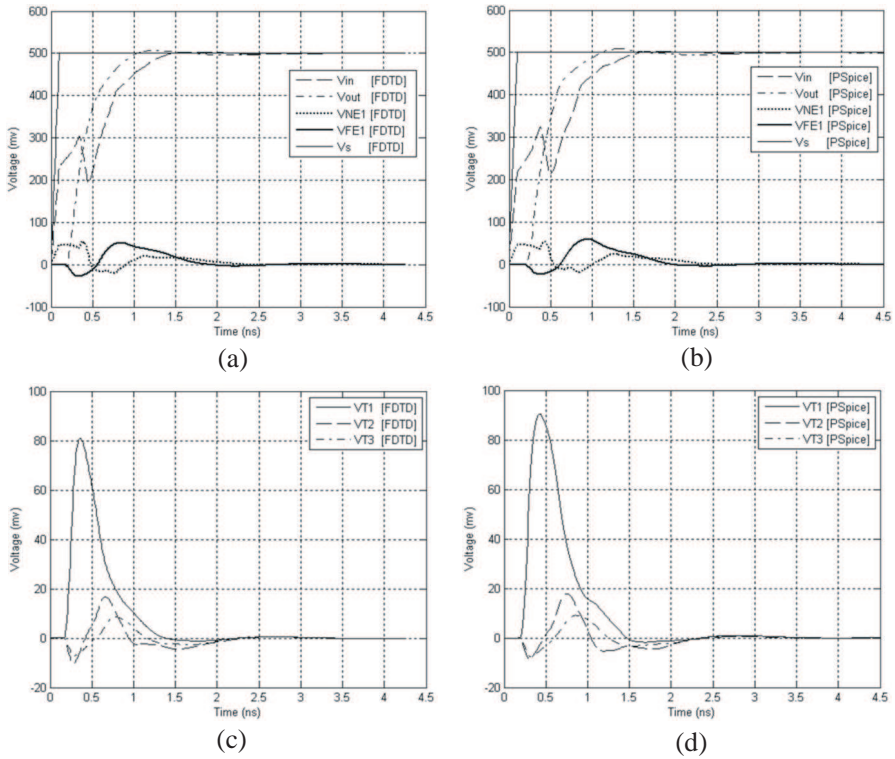
Figure 14. Inputs, outputs and transistors voltage in the case of WB matched multi-MESFETs for the lossless NMTL. (a) FDTD, (b) PSpice, (c) FDTD, and (d) PSpice.
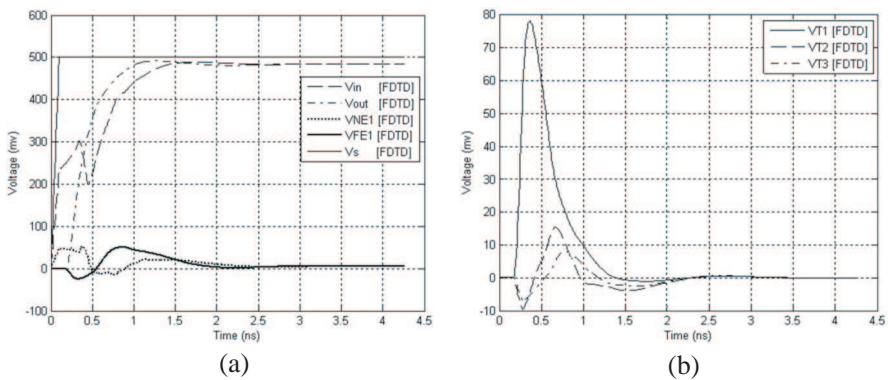

Figure 15. (a) Inputs, outputs voltages and (b) transistor outputs voltages in the case of WB matched multi-MESFETs for the NMTL with frequency dependent loss.

loaded with one MESFET are different from the dimensions of the triangular NMTL in the case of multi-conductors loaded with several MESFETs. It is due to the coupling between conductors.

5. CONCLUSION

The wideband impedance matching of multi-nonlinear load using NMTL, whose section and characteristic impedance change continuously, were described and simulated in transient domain and coupling context. This type of impedance matching, using NMTL, is based on the use of tapered lines. A computational approach based upon the centered-points finite-difference time-domain (FDTD) technique for evaluating voltages and currents along the NMTL with frequency dependent losses (metallic losses and dielectric losses) was developed and used. This technique allows to introduce, easily, multi-nonlinear complex components in the algorithm, as the GaAs MESFETs studied here. A new system of equations describing nonlinear elements in MESFETs, based on matrices was developed. This system of equations was solved by using the Newton-Raphson's method.

Several examples were treated. In all the examples, the WB impedance transformer eliminates the overshoot and the distortions, due to the elimination of reflections. As a result, it reduces the settling time of the circuit.

The results of the simulation with FDTD method have been compared to those obtained in PSpice, in the case of one conductor plus the reference conductor, connected to linear element (resistance), in the case of one conductor and a reference conductor, connected to strongly nonlinear element (one GaAs MESFET) and in the case of six (including the reference conductor), frequency dependent, lossless and lossy nonuniform conductors connected to strongly nonlinear elements (five GaAs MESFETs). A good level of agreement has been achieved.

In addition to being very flexible in treating nonuniform lines (can deal with arbitrary NMTL) and frequency dependent losses, the proposed method has no limitation in the number of conductors (compared to some software). Moreover, the CPU time of this approach is less than the conventional time-domain to frequency-domain (TDFD) solution technique.

REFERENCES

1. Collin, R. E., *Foundations for Microwave Engineering*, McGraw-Hill, 1996.

2. Pozar, D. M., *Microwave Engineering,* John Wiley & Sons, 1990.

3. Liao, S. Y., *Microwave Circuit Analysis and Amplifier Design,* Prentice-Hall, 1987.

4. Ha, T. T., *Solid-State Microwave Amplifier Design,* John Wiley & Sons, 1981.

5. Khalaj-Amirhosseini, M., "Wideband or multiband complex impedance matching using microstrip nonuniform transmission lines," *Progress In Electromagnetics Research*, Vol. 66, 15–25, 2006.

6. Huang, X.-D., X.-H. Jin, and C.-H. Cheng, "Novel impedance matching scheme for patch antennas," *Progress In Electromagnetics Research Letters*, Vol. 14, 155–163, 2010.

7. Zhang, B, "A D-band power amplifier with 30-GHz bandwidth and 4.5-DBM P_{sat} for high-speed communication system," *Progress In Electromagnetics Research*, Vol. 107, 161–178, 2010.

8. Reynolds, S. K., B. A. Floyd, U. R. Pfeiffer, T. Beukema, J. Grzyb, C. Haymes, B. Gaucher, and M. Soyuer, "A silicon 60-GHz receiver and transmitter chipset for broadband communications," *IEEE J. Solid-State Circuits*, Vol. 41, No. 12, 2820–2831, Dec. 2006.

9. Powell, J., H. Kim, and C. G. Sodini, "SiGe receiver front ends for millimeter-wave passive imaging," *IEEE Trans. Microw. Theory Tech.*, Vol. 56, No. 11, 2416–2425, Nov. 2008.

10. Nicolson, S. T., A. Tomkins, K. W. Tang, A. Cathelin, D. Belot, and S. P. Voinigescu, "A 1.2 V, 140 GHz receiver with on-die antenna in 65 nm CMOS," *IEEE Radio Frequency Integrated Circuits Symposium*, 229–232, Jun. 2008.

11. Lin, Y.-J., S. S. H. Hsu, J.-D. Jin, and C. Y. Chan, "A 3.1–10.6 GHz ultra-wideband CMOS low noise amplifier with current-reused technique," *IEEE Microwave and Wireless Components Letters*, Vol. 17, No. 3, 232–234, Mar. 2007.

12. Nahman, N. and D. Holt, "Transient analysis of coaxial cables using the skin effect approximation $A + B\sqrt{s}$," *IEEE Tran. on Circuit Theory*, Vol. 19, No. 5, 443–451, Sept. 1972.

13. Yu, Q. and O. Wing, "Computational models of transmission lines with skin effect and dielectric loss," *IEEE Trans. on Circuits And Systems — I: Fundamental Theory and Applications*, Vol. 41, No. 2, 107–119, Feb. 1994.

14. Orlando, A. and C. R. Paul, "FDTD analysis of lossy, multiconductor transmission lines terminated in arbitrary loads," *IEEE Trans. Electromagnetic Comp.*, Vol. 38, No. 3, 388–399,

Aug. 1996.

15. Li, K., M. A. Tassoudji, R. T. Shin, and J. A. Kong, "Simulation of electromagnetic radiation and scattering using a finite difference time domain technique," *Comput. Appl. in Eng. Education*, Vol. 1, No. 1, 45–62, Sept./Oct. 1992.

16. Kabbaj, H. and J. Zimmermann, "Time-domain study of lossy nonuniform multiconductor transmission lines with complex nonlinear loads," *Microwave and Optical Technology Letters*, Vol. 29, No. 5, 296–301, June 2001.

17. Amharech, A. and H. Kabbaj, "Analysis of multiconductor transmission line loaded by multi MESFET transistors modeled by their large signal scheme: An FDTD approach," *International Journal on Communications Antenna and Propagation*, Vol. 1, No. 3, 2011.

18. Kuo, C. N., B. Houshmand, and T. Itoh, "Full-wave analysis of packaged microwave circuits with active and nonlinear devices: An FDTD approach," *IEEE Trans. Microwave Theory Tech.*, Vol. 45, No. 5, 819–826, May 1997.

19. Su, H.-H., C.-W. Kuo, and T. Kitazawa, "A novel approach for modeling diodes into FDTD method," *PIERS Proceedings*, Marrakesh, Morocco, Mar. 20–23, 2011.